


Article

Heterogeneous Activation of Persulfate by Nickel Oxide/Strontium Carbonate Composite for Sulfamethoxazole Degradation in Water

Despoina Jessica Skempi¹, Konstantinos Kouvelis¹, Athanasia Petala², Georgios Bamos^{1,*} 
and Zacharias Frontistis³

¹ Department of Chemical Engineering, University of Patras, GR-26504 Patras, Greece; kozeta007@hotmail.com (D.J.S.); kos_kouv@chemeng.upatras.gr (K.K.)

² Department of Environment, Ionian University, GR-29100 Zakynthos, Greece; apetala@ionio.gr

³ Department of Chemical Engineering, University of Western Macedonia, GR-50132 Kozani, Greece; zfrontistis@uowm.gr

* Correspondence: geoba@chemeng.upatras.gr

Abstract: The development of efficient heterogeneous persulfate activators is one of the main research topics in the wastewater treatment area. The present work deals with the heterogeneous activation of sodium persulfate (SPS) using nickel oxide/strontium carbonate (NiO/SrCO₃) for the degradation of sulfamethoxazole (SMX), a representative compound from the group of antibiotics. Results showed that NiO/SrCO₃ exhibited high performance towards the activation of SPS, leading to SMX elimination in brief time spans. The impact of SPS (25–100 mg/L), NiO/SrCO₃ (50–250 mg/L), and SMX (0.25–3.00 mg/L) concentration, and initial pH on the decomposition of SMX was further examined. Experiments were also conducted in real matrices such as secondary effluent and bottled water, revealing the existence of retarding phenomena compared to ultrapure water. This behavior was further investigated with the addition of bicarbonates, chlorides, or humic acid in ultrapure water. It was found that organic matter significantly hampered SMX removal. The role of the main radicals (hydroxyl and sulfate radicals) was determined using appropriate radical traps (methanol and tert-butanol). These quenching experiments combined with the conducted electrochemical measurements revealed that both a radical and a non-radical mechanism contribute to the decomposition of SMX.

Keywords: persulfate-based advanced oxidation processes (sr-aops); water matrix; catalytic materials; pharmaceuticals; radical and non-radical mechanism



Citation: Skempi, D.J.; Kouvelis, K.; Petala, A.; Bamos, G.; Frontistis, Z. Heterogeneous Activation of Persulfate by Nickel Oxide/Strontium Carbonate Composite for Sulfamethoxazole Degradation in Water. *Environments* **2023**, *10*, 147. <https://doi.org/10.3390/environments10080147>

Academic Editor: Simeone Chianese

Received: 31 July 2023

Revised: 15 August 2023

Accepted: 17 August 2023

Published: 18 August 2023



Copyright: © 2023 by the authors. Licensee MDPI, Basel, Switzerland. This article is an open access article distributed under the terms and conditions of the Creative Commons Attribution (CC BY) license (<https://creativecommons.org/licenses/by/4.0/>).

1. Introduction

Persulfate is a strong oxidizing agent widely used in environmental fields like water purification and soil remediation [1]. In its pure form, persulfate has relatively low reactivity; however, it can be activated, producing sulfate radicals (SO₄^{•−}) characterized by high reactivity and participation in degradation reactions of inorganic and organic pollutants [2]. The desirable characteristics of SO₄^{•−} led to the development of a new subcategory of advanced oxidation processes (AOPs), named sulfate radical-based AOPs (SR-AOPs), where SO₄^{•−} are produced either exclusively or together with hydroxyl radicals [2]. When compared to other AOPs, SR-AOPs offer several advantages such as minimized byproducts formation, ease of application and compatibility with existing infrastructure. In addition, besides its well-documented applications in micropollutants removal from aqueous media, some recent studies have focused on diverse sustainability applications of persulfate technologies. These applications encompass a range of areas, including managing solid waste, extracting metals, and facilitating materials circulation [3,4].

Persulfate can be activated through energy input (thermal, radiation, sonochemical/electrochemical), transition metal ions (iron, cobalt, copper, silver), alkali [5], and

heterogeneous activators [6]. In addition, today sonochemical activation has sparked increasing interest as an alternative activation method. In that case, the ultrasound's energy is not employed directly by the liquid reactants. Instead, the impact of ultrasound occurs via a phenomenon referred to as cavitation. This process encompasses the creation, expansion, and forceful implosion of voids [7,8]. This leads to the development of hybrid systems, such as cavitation combined with photocatalysis, showing enhanced oxidation efficiency [9]. However, among persulfate activation methods, heterogeneous activation appears to be the most effective method, mostly because it has minimal energy requirements, and provides facile separation and reusability of the catalytic materials [10]. The benefit deriving from this fact is twofold. Firstly, the metal leaching observed in homogeneous activation methods is now minimized, and secondly, the operational costs are reduced due to catalyst recovery. In addition, heterogeneous persulfate activation can significantly enhance the overall efficiency of such degradation systems, as the presence of solid catalysts provides additional active sites for persulfate activation. However, it should be noted that heterogeneous catalysts should be characterized by high stability in order to be recovered and reused, reducing their environmental impact.

Numerous investigations have documented the heterogeneous activation of persulfate, and the activation means can be categorized into two main groups: (i) Carbon-based materials, including well-known materials such as activated carbon [11], carbon nanotubes [12], or even graphene [13]. Such materials are considered promising persulfate activators as they provide a high surface area, facilitating the interaction between persulfate and target pollutants [14]; (ii) Catalytic materials such as metal oxides [15], metal phosphides [16], metal-organic frameworks [17] or monolith catalysts with 3D hierarchical structures like δ -MnO₂ immobilized on 3D nickel foam or 3D α -Co(OH)₂ nanosheets developed on robust nickel foam (NF) [18,19]. These catalysts can enhance sulfate radicals production through redox reactions with persulfate, accelerating the oxidation of contaminants [6].

Recently, the development of heterogeneous catalytic materials for persulfate activation has been the focus of research in the water treatment area. Copper, cobalt, and iron oxides have already shown interesting results. For example, elimination of tetracycline in water with the use of a persulfate-activated system was studied by Cao et al., using zero-valent iron [20]. Sulfadiazine, another pharmaceutical degradation, was also successfully achieved using zero-valent iron as a persulfate activator [21]. In addition, nano-zero valent iron immobilized on organo-montmorillonite was synthesized and tested for persulfate activation for sulfamethazine degradation in water [22], while Lei et al. pointed out the advantages deriving from a bimetallic catalytic material, such as CuO-Fe₃O₄, in phenol removal from wastewater [23]. Considering cobalt-based activators, many configurations such as cobalt oxides, cobalt hydroxides, metal-organic frameworks, etc., have been tested and shown promising results [24,25]. However, it is still important to reduce cobalt ion leaching and enhance the stability of such catalytic materials across a wide pH range.

A significant contribution in the field was made by Zhang et al., who studied a CuO/persulfate oxidation system using 2,4-dichlorophenol as the model compound and showed that the peroxydisulfate activation process did not involve SO₄^{•-} generation [26]. In general, the persulfate activation process entails the creation of SO₄^{•-} through electron transfer from the transition metal to persulfate, followed by subsequent reactions between the sulfate radicals and water to form [•]OH. However, in the case of CuO, a non-radical mechanism may take place through reactive complexes formation between persulfate and the activators (such as CuO). A subsequent investigation of the CuO/persulfate system resolved previous observations and indicated that there may be a blend of radical and non-radical mechanisms taking place [27].

However, apart from these well-studied transition metals, the activity of other metal-based catalytic materials remains scarcely reported. Specifically, considering nickel-based catalytic materials that are widely adopted in typical catalytic processes, there are only a very few studies dealing with their use as heterogeneous persulfate activators. In particular, Jiang et al. synthesized nickel stannate-reduced graphene oxide (Ni₂SnO₄-RGO) compos-

ites and incorporated them in a heterogeneous activation persulfate system for bisphenol A degradation in water. Experiments carried out with appropriate radical scavengers showed that both $\text{SO}_4^{\bullet-}$ and $\bullet\text{OH}$ participate in degradation reactions, with the former playing the leading role [28]. Another group studied the efficiency of $\text{Ni}_x\text{Co}_{3-x}\text{O}_4$ for the bisphenol A and tetracycline decomposition. The researcher found that it possesses higher efficiency than NiO and Co_2O_3 [29]. Moreover, nickel was mixed with lanthanum oxide, forming perovskite phases showing appreciable activity and stability. Very recently, Kim et al. demonstrated a non-radical activation mechanism in the case of Ni–NiO nanocomposites [30]. Furthermore, oxygen vacancies-rich NiO could activate persulfate by a non-radical mechanism leading to a fast phenol elimination [31]; this hypothesis was further verified by Xie et al., studying sulfamethoxazole degradation in water using pompon-like NiO microspheres as a heterogeneous persulfate activator [32].

On the other hand, many researchers stated that the persulfate activation mechanism in the case of NiO should include $\text{SO}_4^{\bullet-}$ formation, as the $\text{Ni}^{2+}/\text{Ni}^{3+}$ redox potential allowed Ni^{2+} to react with persulfate generating $\text{SO}_4^{\bullet-}$ [33–35].

The above-mentioned contradictory conclusions regarding the use of NiO as a heterogeneous persulfate activator indicate the need for further research. Within this framework, NiO/ SrCO_3 was chosen as the heterogeneous persulfate activator in this study. Considering strontium-based materials, Gkika et al. investigated sulfamethoxazole degradation in water with the use of lanthanum strontium cobaltite perovskite oxide [36], whereas Miao et al. synthesized $\text{SrCo}_{1-x}\text{Ti}_x\text{O}_{3-\delta}$ perovskite oxides and reported their efficiency towards persulfate activation for phenol degradation [37]. In addition, strontium has been used as a promoter in different catalytic configurations, such as BiFeO_3 [38] and LaFeO_3 [39].

This is the first time that such a catalytic configuration has been used for persulfate activation. The ability of NiO/ SrCO_3 to activate SPS was investigated in terms of degrading the antibiotic sulfamethoxazole (SMX) in ultrapure water (UPW). SMX has been detected in concentrations ranging from nanograms per liter to milligrams per liter in treated effluents [40,41]. The persistence of SMX in the environment can lead to potential ecological harm, as it may disrupt the balance of aquatic ecosystems, affecting various organisms, including algae, fish, and other aquatic life. Moreover, it can boost the growth of antibiotic resistance in bacteria, having fatal implications for human health [42].

NiO/ SrCO_3 was synthesized following a combustion method, while BET, XRD, and TEM techniques were used for the catalyst characterization. The effectiveness of the NiO/ SrCO_3 /SPS system for SMX removal was reported not only in ultrapure water (UPW) but also in real and synthetic water matrices, such as treated effluent (WW) and bottled water (BW).

2. Materials and Methods

2.1. Chemicals and Aqueous Media

Table 1 summarizes the chemicals (Sigma Aldrich, Merck KGaA, Darmstadt, Germany and/or its affiliates) used in this work.

Table 1. Chemicals employed in this work.

Name	Formula	CAS Number
Sulfamethoxazole, SMX	$\text{C}_{10}\text{H}_{11}\text{N}_3\text{O}_3\text{S}$	723-46-6
Sodium persulfate, SPS	$\text{Na}_2\text{S}_2\text{O}_8$	7775-27-1
Methanol	CH_3OH	67-56-1
Sulfuric acid	H_2SO_4	7664-93-9
Sodium hydroxide	NaOH	1310-73-2
Sodium bicarbonate	NaHCO_3	144-55-8
Sodium chloride	NaCl	7647-14-5

Table 1. *Cont.*

Name	Formula	CAS Number
Humic acid	-	1415-93-6
Tert-butanol	(CH ₃) ₃ COH	75-65-0
Strontium nitrate, 99.995% trace metals basis	Sr(NO ₃) ₂	10042-76-9
Nickel (II) nitrate hexahydrate, 99.999% trace metals basis	Ni(NO ₃) ₂ ·6H ₂ O	13478-00-7
Citric acid	C ₆ H ₈ O ₇	77-92-9
Ammonium nitrate	NH ₄ NO ₃	6484-52-2
Ammonia	NH ₃	7664-41-7

In the majority of the experiments presented in this study, ultrapure water (UPW, Millipore Milli-Q Gradient A10) was used as the water matrix. However, in some experiments, treated effluent (WW) from the wastewater treatment plant of the University of Patras and commercially available bottled water (BW) were examined as environmental matrices. The physicochemical characterization of aqueous matrices is shown in Table 2.

Table 2. Water matrices' characteristics.

Parameter	WW	BB	UPW
pH	8	7.5	6
Conductivity [μS/cm]	0.33	0.39	0.012
Alkalinity [mg/L]	190	152	-
Sulfates [mg/L]	33	15	-
Chlorides [mg/L]	69	9.8	-
Bicarbonates [mg/L]	190	209	-
TOC [mg/L]	7	-	-
COD [mg/L]	21	-	-

2.2. NiO/SrCO₃ Synthesis

The preparation of NiO/SrCO₃ took place by the in situ ignition method [43]. First, the precursor compounds Sr(NO₃)₂ and Ni(NO₃)₂ were diluted under stirring to triple distilled water. Then, a solution of citric acid, C₆H₈O₇, and ammonium nitrate, NH₄NO₃, was added and the solution was continuously stirred. Appropriate amounts of NH₃ were added (pH = 9) in order to neutralize the excess of citric acid, followed by heating through the hot plate under stirring.

When the water had evaporated, the container was heated vertically and circumferentially using a heat gun from a distance of 5 cm.

The mixture ignited into a thin crust and crumbled into a fine powder. Finally, it was calcined in air for 5 h at 700 °C [44]. The obtained wt.% of NiO was equal to ca. 33.

2.3. NiO/SrCO₃ Physicochemical Characterization Techniques

The crystal structure of NiO/SrCO₃ was examined using X-ray diffraction (XRD) through an A Bruker D8 Advance device (Billerica, MA, USA) equipped with a Cu Kα source (wavelength λ = 1.5496 Å). For the purpose of capturing transmission electron microscopy (TEM) images, a JEOL JEM-2100 system (Tokyo, Japan) at 200 kV was employed, offering a resolution of 0.23 nm for point measurements and 0.14 nm for lattice measurements. The specific surface area (SSA) was estimated using the Brunauer–Emmett–Teller (BET) method, employing a Gemini III 2375 instrument from Micromeritics [45].

2.4. Analytical Methods and Experimental Procedures

The SMX oxidation was investigated within a 250 mL cylindrical Pyrex reaction container exposed to the atmosphere. At first, the vessel was loaded with a solution (volume 120 mL) with the selected concentration of SMX, followed by the addition of pre-measured SPS and NiO/SrCO₃ loading. The degradation tests were performed at 25 °C without regulating the solution's pH, and continuous magnetic stirring was maintained throughout the process.

To analyze the samples, 1.2 mL portions were withdrawn from the vessel at specific times. These samples were mixed with methanol to stop the reaction, filtered, and subjected to analysis using high-performance liquid chromatography (HPLC). The HPLC system utilized for this purpose consisted of an Alliance 2695 HPLC system connected with a Waters 2996 photodiode array detector. Separation was achieved using a Kinetex column (C18 100A, 150 mm × 3 mm; 2.6 μm particle size, Phenomenex (Torrance, CA, USA) thermostated at 45 °C.

For the investigation of the combined activation of persulfate by NiO/SrCO₃ and simulated solar light irradiation, additional tests were performed using an Oriel, LCS-100 solar simulator equipped with a 100 W Xenon arc lamp.

2.5. Electrochemical Characterization

2.5.1. Electrochemical Measurements

Electrochemical analysis was carried out implementing an PGSTAT128N Auto lab potentiostat (Utrecht, The Netherlands) at room temperature (ca. 25 °C) in a three-electrode setup using 0.1 M Na₂SO₄ as the electrolyte, while a Ag/AgCl (3 M KCl) purchased from (Metrohm A.G., Herisau, Switzerland) served as the reference electrode and a Pt wire served as the counter electrode. The working anodic electrode was the examined NiO/SrCO₃ material deposited on FTO (NiO/SrCO₃/FTO), whose preparation is described in detail in the following section. Electrochemical impedance spectroscopy (EIS) and linear sweep voltammetry (LSV) measurements were performed in order to examine the potential effect of an electron transfer mechanism to SMX elimination [46,47]. LSV and EIS experiments were performed using the electrolyte solution of only the examined catalyst (NiO/SrCO₃/FTO), with the presence of the catalyst and amount of SPS as well as when in the presence of the catalyst and amounts of SPS and SMX. LSV curves were obtained by scanning linearly the applied potential from the open circuit potential (OCP) value (−0.2 V vs. Ag/AgCl) to 1.5 V vs. Ag/AgCl applying a potential scan rate equal to 50 mV s^{−1} whereas EIS data were recorded under OCP conditions in the frequency range 0.1 to 100 kHz and with an amplitude perturbation of 0.01 V.

2.5.2. Synthesis of NiO/SrCO₃/FTO Working Electrode

The NiO/SrCO₃ was immobilized as a thin film on a coated glass of high conductive fluorine—doped tin oxide. The deposition was performed employing a suspension of 100 mg NiO/SrCO₃, 1.2 mL ethanol and 0.4 mL of 5 wt.% Nafion[®] ionomer solution (Sigma Aldrich, St. Louis, MO, USA). The mixture was ultrasonicated for 30 min in a sonochemical bath (Bandelin electronic GmbH & Co. KG, Berlin, Germany) in order to obtain the desired homogeneity [48]. The Nafion solution was used for electrode stability enhancement and maintenance of the thin film uniformity. The deposition of the aforementioned suspension on the FTO surface was performed via drop-casting and subsequent drying overnight at 75 °C. The prepared electrode surface area and the resulting areal density were ca. 1 cm² and 10 mg/cm², respectively.

3. Results and Discussion

3.1. Physicochemical Characterization

Figure 1 shows the X-ray diffraction spectrum of the NiO/SrCO₃ sample. It is observed that the spectrum consists of peaks corresponding to the SrCO₃ orthorhombic structure (JCPDS No 05-0418). Furthermore, the peaks at 37.4° and 43.5° correspond to NiO (JCPDS No. 1-1239), verifying the successful formation of the composite material. The SSA of NiO/SrCO₃ was estimated at ca. 5 m²/g.

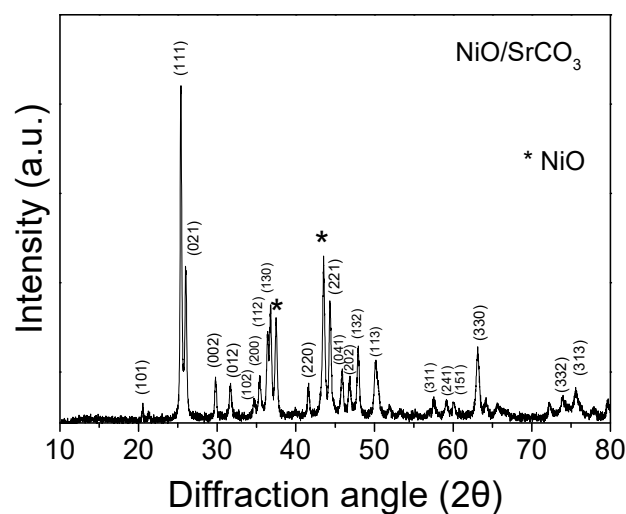


Figure 1. XRD pattern of NiO/SrCO₃.

The morphology together with the particle size of the as prepared material was further investigated by TEM images (Figure 2). It was observed that NiO/SrCO₃ is made up of spherical-like nanoparticles with an estimated average diameter of approximately 31 nm (Figure 2C). Moreover, it could be stated that the particle size distribution (Figure 2C) is rather broad, including particles from 10 to ca. 65 nm.

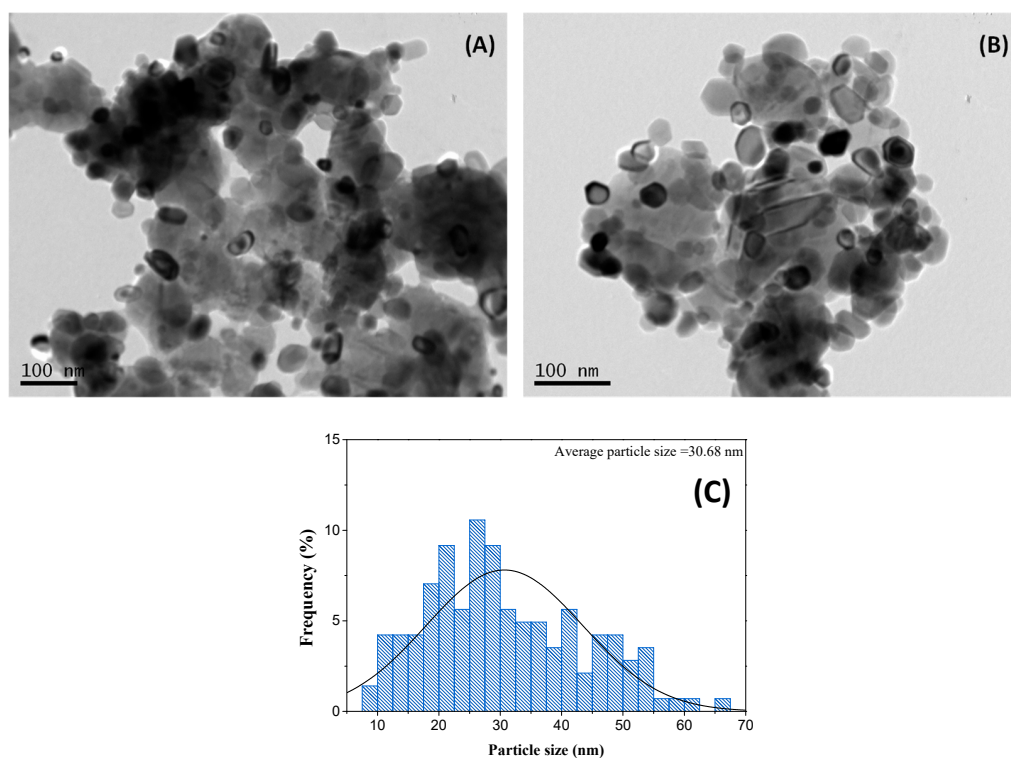


Figure 2. (A,B) TEM images and (C) particle size distribution of NiO/SrCO₃.

3.2. Effect of Experimental Conditions on SMX Removal in the NiO/SrCO₃/SPS System

In the domain of SR-AOPs, the ability of nickel oxide (NiO) to activate sodium persulfate (SPS) efficiently has exhibited inherent limitations, thereby compelling researchers to seek diverse modifications to enhance its efficacy [30,49]. Acknowledging this significant challenge, the present scientific study endeavors to address this limitation by fabricating a novel composite material that combines nickel oxide with strontium carbonate (NiO/SrCO₃). The primary

objective of this synthesis is to achieve successful activation of SPS for the SMX elimination. Because the latter serves as a representative antibiotic compound, the proposed system could offer a promising approach to environmental remediation.

In the preliminary stage of our research effort, a thorough investigation was conducted to scrutinize the impact of crucial operating parameters, like catalyst loading, SPS concentration, SMX concentration, and the solution initial pH. It is important to highlight that according to the literature, the reaction is governed by pseudo-first-order kinetics [50–52].

3.2.1. Impact of SPS Concentration on the Degradation Reaction

To explore the influence of SPS loading on the oxidation process and effectively eliminate 500 µg/L of SMX, a series of experiments was conducted, gradually increasing the SPS dosage from 0 to 100 mg/L. Throughout these experiments, 100 mg/L of catalyst was employed. The reactions were carried out in ultra-pure water (UPW) at room temperature.

Initially, the adsorption of SMX on the surface of the composite catalyst in the absence of SPS was quantified, and it was found to be negligible, causing only a minor decrease in SMX concentration (less than 5%). This finding could be correlated with the diminutive specific surface area of NiO/SrCO₃ (5 m²/g). However, as shown in Figure 3a, upon increasing the SPS dosage to 50 mg/L, a remarkable enhancement in the degradation reaction rate was observed. In particular, complete elimination of SMX was achieved within 45 min, while the apparent reaction rate constant (k_{app}) presented a notable threefold increase (from 0.032 min⁻¹ to 0.092 min⁻¹). Interestingly, when the loading of SPS was further increased to 100 mg/L, SMX degradation was not favored, coinciding with a slight decrease in k_{app} value from 0.092 to 0.068 min⁻¹. This observation can be attributed to the self-quenching, or the scavenging of the reactive species from SPS. Specifically, the generated sulfate radicals (SO₄^{•-}) may undergo self-recombination or react with SPS molecules instead of effectively reacting with the organic compounds according to Equations (1) and (2) [53,54]:

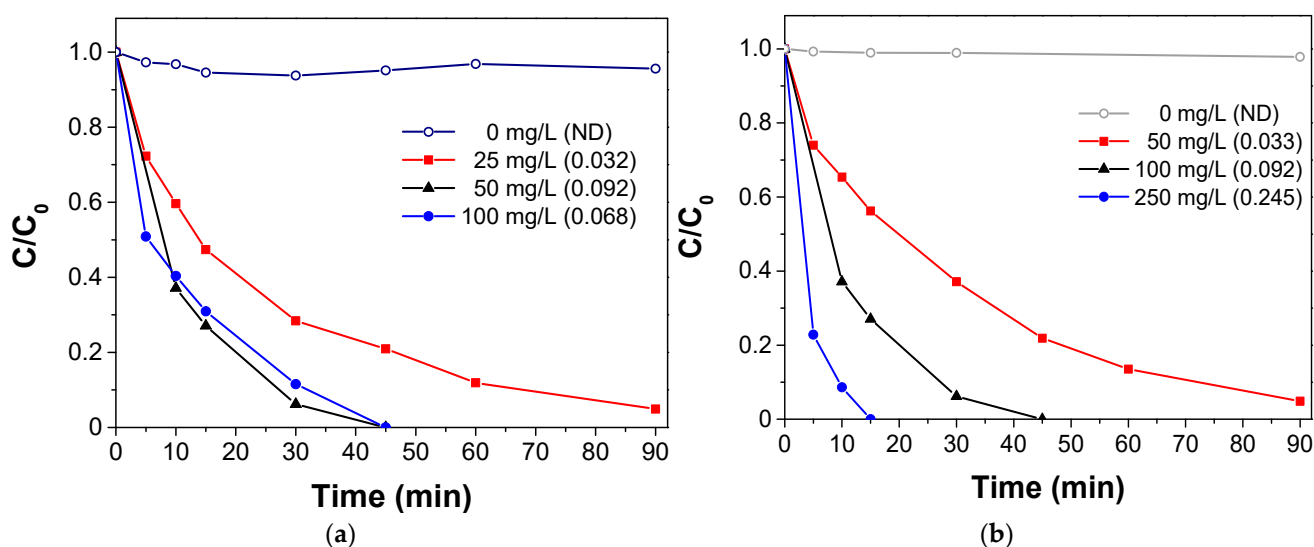


Figure 3. Effect of (a) SPS concentration (b) catalyst dosage on the removal of 0.5 mg/L SMX.

The above results are in the same order of magnitude as others obtained in similar systems for SMX degradation [4]. Based on the results obtained in Figure 3a, a [SPS] = 50 mg/L was chosen for the following tests.

3.2.2. Effect of NiO/SrCO₃ Dosage

The effect of the catalyst was evaluated by ranging the loading from 0 to 250 mg/L while maintaining the loading of SPS constant at 50 mg/L. As depicted in Figure 3b, the inherent oxidizing potential of SPS, in the absence of the catalyst, proved to be insignificant, aligning with the findings reported in prior studies [36,55]. The progressive increase in NiO/SrCO₃ dosage from 50 to 250 mg/L engendered a noteworthy increase in the degradation rate, as evidenced by the removal efficiencies of SMX after 15 min, which were 44%, 73%, and 100%, respectively. The most probable rationale behind this observation is that the higher NiO/SrCO₃ concentration provides a higher number of active sites for SPS activation, resulting in an increased population of reactive species [54–56]. Despite obtaining optimal results at a catalyst dosage of 250 mg/L, subsequent experiments were performed at 100 mg/L, with the aim of conserving the catalyst usage.

3.2.3. Effect of Antibiotic Concentration

The effect of the antibiotic loading was comprehensively assessed through a set of experiments performed at four distinct SMX loadings (0.25–3.00 mg/L), and the corresponding normalized concentration versus time profiles are presented in Figure 4a. The removal process was substantially hindered as the SMX concentration was raised. Specifically, at the 30-min mark, the removal efficiencies in each case were as follows: 100% for 0.25 mg/L, 93% for 0.50 mg/L, 70% for 1.00 mg/L, and 20% for 3.00 mg/L. From the perspective of kinetics, the corresponding k_{app} values are 0.116, 0.092, 0.037, and 0.004 min⁻¹, confirming the deviation from a true first-order model, since the kinetic constant is contingent on initial SMX concentration. The reason behind this observation is the fact that under defined operating parameters (e.g., catalyst loading, SPS concentration, solution pH, temperature), the population of the reactive species (mainly free radicals) remains practically constant while the concentration of the organic compound is steadily increasing, demanding longer time periods for the same extent of degradation [12].

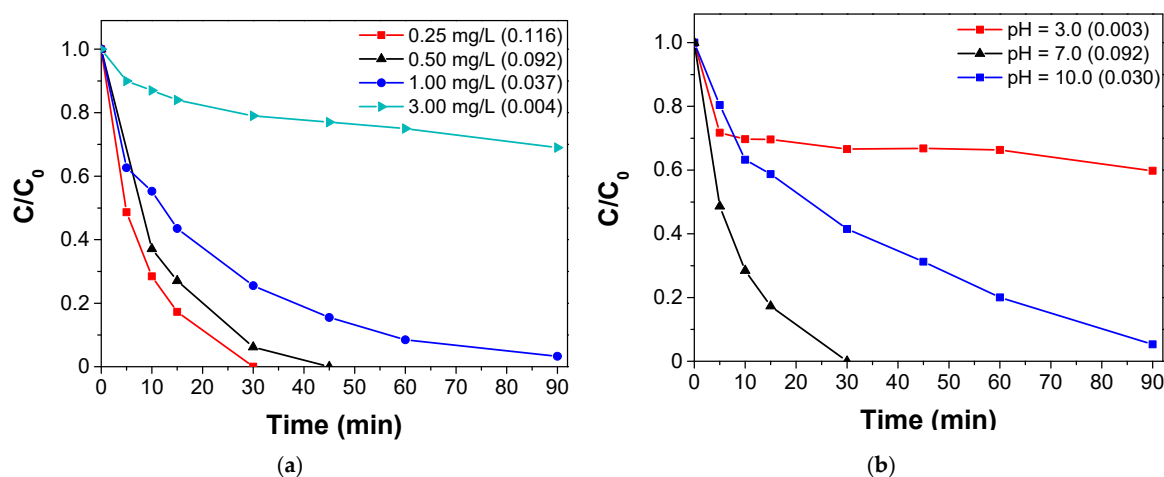


Figure 4. Removal profiles of SMX as a function of (a) initial SMX concentration; (b) initial solution pH ([SMX] = 0.5 mg/L). Experimental conditions: [Catalyst] = 100 mg/L, [SPS] = 50 mg/L.

3.2.4. Effect of pH

Solution's pH is an essential factor that exerts substantial influence on the removal of organic compounds in a catalyst/SPS system. To thoroughly investigate its impact, a set of experiments was conducted, encompassing a range of pH conditions, spanning from acidic (pH 3) to neutral (pH 7) and alkaline environments (pH 10). According to Figure 4b, a neutral environment proved to be more conducive to the abatement of SMX compared to acidic and alkaline conditions. In the neutral pH setting, complete elimination of SMX was attained within 30 min, whereas the removal efficiencies in the acidic and alkaline cases reached only 30% and 40% in the same time period.

To further elucidate these results, both the catalyst's surface charge and the prevailing chemical form of SMX should be clarified. According to scientific reports, the reported pKa values of the SMX are 1.7 and 5.5 [57]. At a pH value of 3, SMX retains its molecular structure, whereas at pH 7 and 10, it undergoes deprotonation, promoting negatively charged species formation. Having in mind the collected data, it is reasonable to infer that at pH 10, repulsive interactions likely developed between SMX and the NiO/SrCO₃ surface. Consequently, SMX encounters hindrances in reaching the catalyst's surface, leading to limited SMX degradation. In contrast, under strong acidic environments, it has been reported that persulfate may be consumed, as described in Equation 3, resulting in the observed slow removal rate [51,58].



3.2.5. Impact of Water Matrix and Additives on Process Efficiency

In the subsequent phase of our study, assays were carried out to gain knowledge into the implementation of the NiO/SrCO₃/SPS system under different water matrices. As practical applications of SPS-based AOPs are still limited, it becomes essential to interpret how the complexity of the water matrices affects the effectiveness of the catalytic system. To explore this aspect, two distinct water sources were utilized: BW and WW. Results are summarized in Figure 5a.

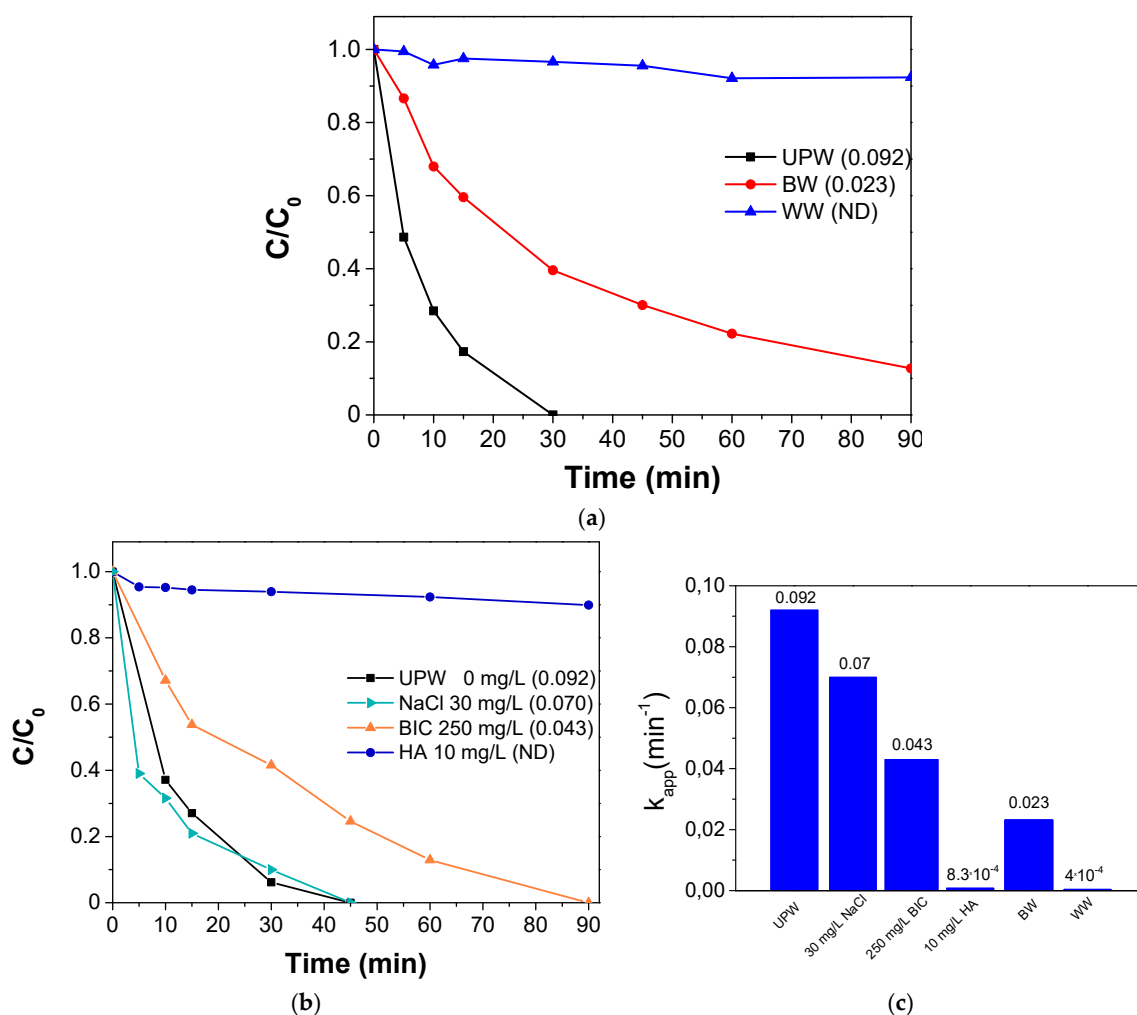


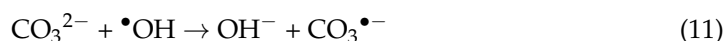
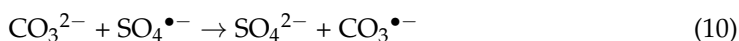
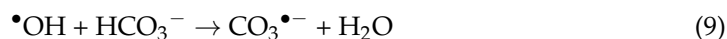
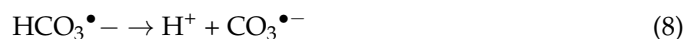
Figure 5. Effect of (a) water matrix (b) inorganic anions and organic matter on SMX degradation. (c) Apparent rate constant (k_{app}) values. Experimental conditions: [Catalyst] = 100 mg/L, [SPS] = 50 mg/L, [SMX] = 0.5 mg/L.

The experimental findings clearly demonstrate that elevating water matrix's complexity exerts a significantly adverse impact on SMX degradation. The SMX removal is 60% in BW and does not exceed 5% in WW after 30 min of reaction. The observed reaction rates are markedly decreased, likely due to the presence of ions which can either act as scavengers, consuming the generated free radicals, or they could potentially be a competitor with the antibiotic, thereby masking the catalyst's active sites [59,60]. In the case of WW, the inhibitory effects are clearly pronounced, presumably due to the existence of organic matter.

Further tests were conducted in artificial matrices enriched with predetermined amounts of sodium chloride (NaCl 30 mg/L), bicarbonates (HCO_3^- 250 mg/L), and humic acid (HA 10 mg/L). HCO_3^- and Cl^- were specifically selected because they are the dominant components in BW. On the other hand, HA was used as a representative compound accurately imitating the organic moieties detected in treated effluent or environmental samples. Figure 5b reveals that the addition of 30 mg/L NaCl has a minor impact on the oxidation, leading to a slight reduction in the k_{app} value from 0.092 to 0.070 min^{-1} . This phenomenon may be probably attributed to the interaction between the reactive species and the chlorine ions, leading to the formation of chlorine radicals as expressed in Equations (4)–(6) [50,61]:



Figure 5b highlights the negative effect of bicarbonates on the oxidation of SMX. Specifically, the addition of 250 mg/L HCO_3^- (representative BIC concentration in BW) induced a two-fold decrease in k_{app} values, compared to the experiment conducted in UPW, extending the complete breakdown time of SMX to 90 min. The presence of BIC initiated side reactions, consuming the highly reactive free radicals ($\text{SO}_4^{\bullet-}$, $\bullet\text{OH}$) and led to the subsequent creation of secondary species with reduced potential, as described in the following Equations (7)–(11) [16,62]. Additionally, BIC facilitated the development of a strong alkaline environment ($\text{pH} = 9$) which was previously noted to impede the oxidation reaction. In fact, the majority of documented research is conducted using ultrapure water, which overlooks the interplay between organic and inorganic substances such as carbonates and reactive oxygen species. This leads to inaccurately high yields that do not reflect the real outcomes. On a positive note, certain recent investigations have taken into account the matrix impact on the degradation of micropollutants [63].



Regarding HA, it is evident that it completely suppressed the oxidation of SMX (Figure 5b,c), as SMX removal does not exceed 10% and k_{app} values were nearly identical to those observed in experiments performed in WW. HA competes with SMX, quenching the free radicals through its aromatic groups. Furthermore, it has been reported that HA is able to cover the catalyst's surface, obstructing active sites and thereby impeding the activation of SPS [55,64].

3.3. Degradation Mechanism

3.3.1. Electrochemical Measurements

Figure 6 presents the electrochemical characteristics of the NiO/SrCO₃/FTO electrode. The measured current (mA), as demonstrated in Figure 6a, may practically refer to current density (mA cm⁻²) since the surface area of the working electrode is equal to 1 cm². It is obvious from the LSV curves shown in Figure 6a that adding 50 mg L⁻¹ SPS in the electrolyte solution increased the current, which could be attributed to the formation of metastable reactive complexes thus facilitating the SPS and active catalytic surface interaction [46]. Specifically, the maximum current density enhanced from approximately 1 mA cm⁻² when the Ni/SrCO₃ was present in the electrochemical system to approximately 1.8 mA cm⁻² in the case of the Ni/SrCO₃/SPS system. The same behavior was observed with the addition of the SMX pollutant (0.5 mg L⁻¹) in the electrolyte solution. The measured current values increased further (above 2 mA cm⁻²) with the co-presence of the NiO/SrCO₃, SPS, and SMX) in the Na₂SO₄ solution, implying an electron transfer mechanism on the interface of NiO/SrCO₃/FTO, SPS, and SMX.

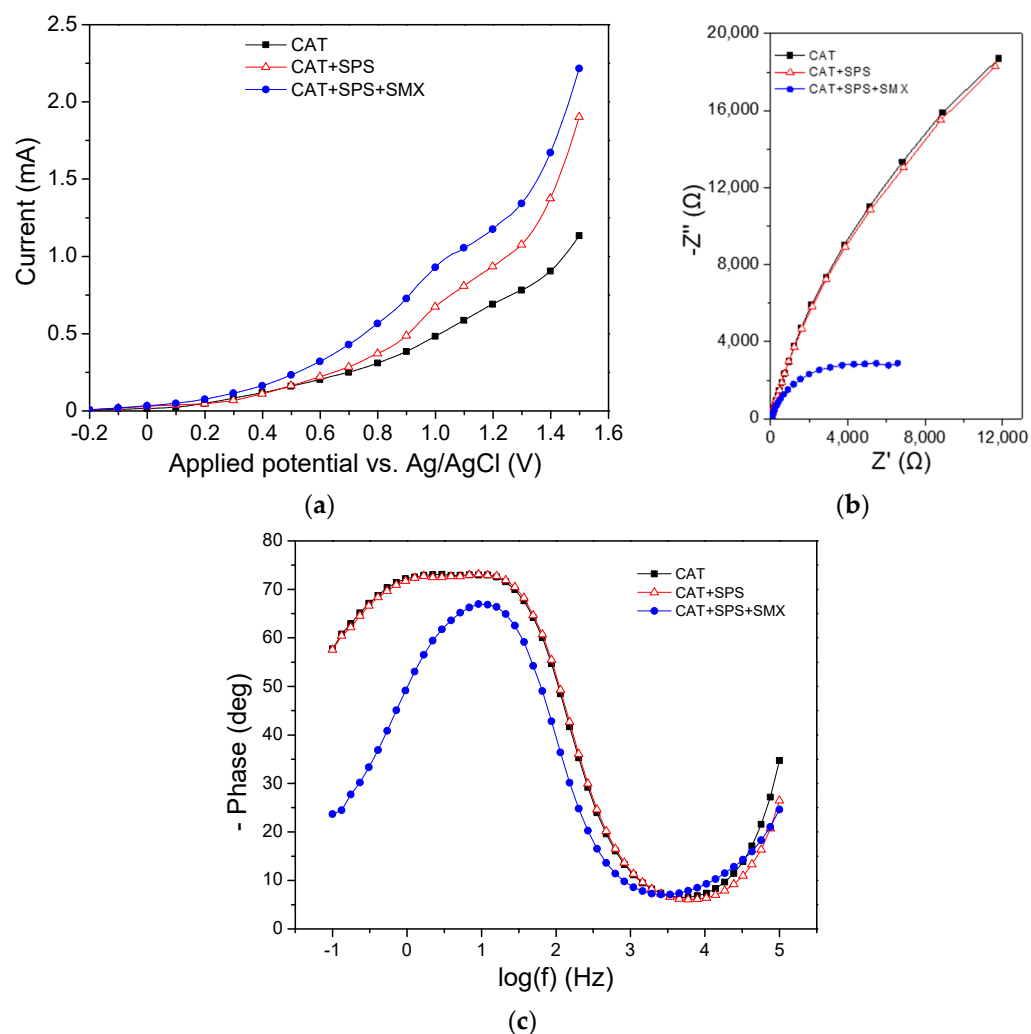


Figure 6. (a) Linear sweep voltammograms and EIS characteristics depicted in the form of (b) Nyquist plots and (c) Bode plots recorded in the presence of catalyst (CAT) and in the co-presence of catalyst (Ni/SrCO₃) and SPS (CAT + SPS) as well as catalyst, SPS and SMX (CAT + SPS + SMX); Measurements were conducted in a three-electrode set-up with the Ni/SrCO₃/FTO as working electrode, a Ag/AgCl (3M KCl sat.) as reference electrode and a Pt wire as counter electrode. Open circuit potential: -0.2 V vs. Ag/AgCl.

The behavior of the LSVs was reflected in the EIS characteristics as depicted in Figure 6b,c. Figure 6b shows the Nyquist plots as recorded in the aforementioned three scenarios. The calculation of the charge transfer resistance, RCT, cannot be performed since the semicircles are incomplete. However, it is evident that the addition of SPS and SMX decreased the semicircle diameter, which is more evident in the NiO/SrCO₃/SPS/SMX system, indicating higher electrical conductivity. This observation is reflected in the shape of the Bode plots as demonstrated in Figure 6c. A reduction in the intensity of the peaks of the Bode plots was observed when comparing the electrochemical system without and in the presence of SMX, which was accompanied by shifting the peak's maximum towards higher frequencies indicating a decline of the characteristic relaxation time of the examined electrochemical system. The appearance of a flattened semicircle in the Nyquist plots and a main peak in the Bode plots implies the realization of a dominant process which could be mainly related to the charge transfer resistance, whereas various subprocesses that may take place simultaneously in the electrochemical system cannot be distinguished. In any case, the appearance of a flattened semicircle implies that the processes that occur are intertwined and overlap with each other, while a dominant process is essentially the one which controls the reaction rate and subsequently the NiO/SrCO₃ performance towards SMX degradation.

It can be concluded that the simultaneous presence of NiO/SrCO₃/FTO, SPS, and SMX led to an increment in the measured current values when the potential changing and to a RCT decline, implying SMX oxidation via a non-specific pathway. In particular, it can be assumed that the SMX oxidation may occur via electron transfer from the organic compound acting as an electron donor, to SPS acting as an electron acceptor) mediated by the NiO/SrCO₃ catalyst [46,65].

3.3.2. Scavengers of Reactive Species

To investigate the reactive species involved in the oxidation of SMX, quenching experiments were conducted utilizing the appropriate scavengers. In this regard, methanol (MeOH, 5 g/L) and tert-butanol (TBA, 5 g/L) were employed to trap SO₄^{•-} ($k = 3.2 \times 10^6 \text{ M}^{-1} \text{ s}^{-1}$) and [•]OH ($k = 3.8\text{--}7.6 \times 10^8 \text{ M}^{-1} \text{ s}^{-1}$), respectively. It should be mentioned that MeOH also interacts with [•]OH ($k = 3.0 \times 10^8 \text{ M}^{-1} \text{ s}^{-1}$) [66].

The outcomes from Figure 7a clearly indicate the significant contribution of hydroxyl radicals as the dominant radical since the oxidation rate was substantially decreased when TBA was added. Contrarily, the contribution of SO₄^{•-} appears to be minor, as the addition of MeOH leads to a negligible differentiation in k_{app} value compared to the experiments with TBA (Figure 7b).

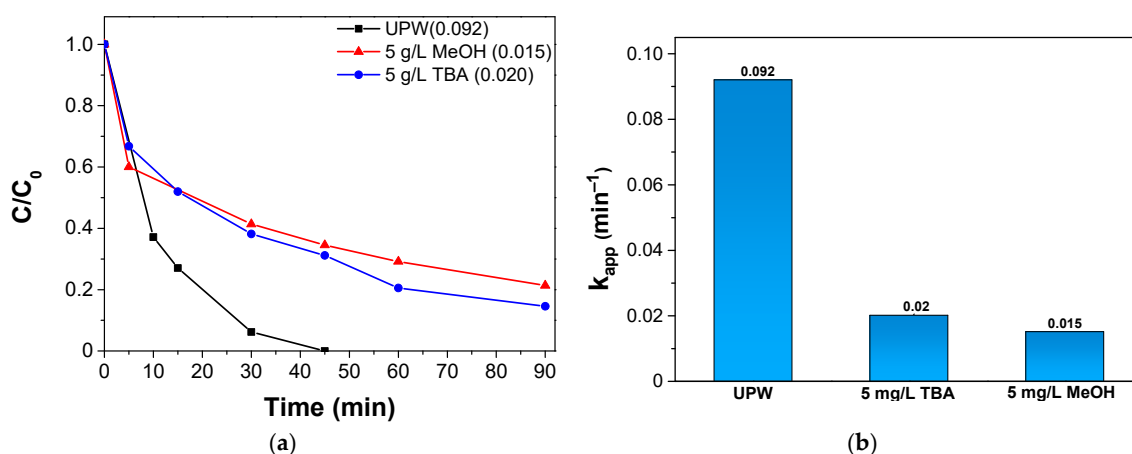


Figure 7. (a) Effect of quenching agents on the oxidation of 0.5 mg/L SMX; (b) Apparent rate constant (k_{app}) values. Experimental conditions: [Catalyst] = 100 mg/L, [SPS] = 50 mg/L, [TBA] = 5 g/L, [MeOH] = 5 g/L.

Overall, based on the data collected from the electrochemical characterization and trapping experiments, it can be strongly suggested that the successful oxidation of SMX involves a combination of non-radical and radical mechanisms.

4. Conclusions

This study focused on the development of a novel NiO/SrCO₃ catalytic material for SMX elimination via SPS activation. This catalytic system was prepared using the combustion method, and its physicochemical characteristics were examined through various methods. The composite material demonstrated exceptional catalytic activity, as complete decomposition of SMX was achieved in short time periods in UPW (45 min). The SMX degradation was described by pseudo first-order kinetics, while the apparent kinetic constant decreased with SMX concentration. SMX degradation was favored at pH 7. A significant inhibition was observed in the test performed in environmental matrices such as secondary effluent or bottled water, possibly due to competition from matrix constituents for reactive species and the surface area, as demonstrated in the experiments conducted in the presence of humic acid or bicarbonates. Notably, chlorides in concentrations up to 30 mg/L did not significantly alter the kinetics. Based on the electrochemical and scavenging measurements, it could be concluded that SMX degradation may occur via both radical and non-radical pathways. Overall, the examined system showed promising results for the decomposition of SMX. However, future studies must assess the catalyst reuse through operation under continuous flow, and further examine the mechanistic aspects of the system, including the study of the transformation by-products and their toxicity.

Author Contributions: Conceptualization, A.P. and Z.F.; Writing, A.P., K.K. and G.B.; writing—review and editing, Z.F.; Investigation, D.J.S., G.B. and K.K.; Methodology, D.J.S. and K.K.; Supervision, Z.F. and A.P. All authors have read and agreed to the published version of the manuscript.

Funding: This work is funded by the project Development of New Innovative Low Carbon Footprint Energy Technologies to Enhance Excellence in the Region of Western Macedonia (MIS 5047197), which is implemented under the Action “Reinforcement of the Research and Innovation Infrastructure”, funded by the Operational Program “Competitiveness, Entrepreneurship and Innovation” (NSRF 2014-2020) and co-financed by Greece and the European Union (European Regional Development Fund).

Data Availability Statement: Not applicable.

Acknowledgments: The authors wish to thank M. Kollia staff in the Laboratory of Electron Microscopy and Microanalysis (L.E.M.M.) at the University of Patras for TEM images.

Conflicts of Interest: The authors declare no conflict of interest.

References

1. Domingues, E.; Silva, M.J.; Vaz, T.; Gomes, J.; Martins, R.C. Persulfate Process Activated by Homogeneous and Heterogeneous Catalysts for Synthetic Olive Mill Wastewater Treatment. *Water* **2021**, *13*, 3010. [\[CrossRef\]](#)
2. Giannakis, S.; Lin, K.Y.A.; Ghanbari, F. A Review of the Recent Advances on the Treatment of Industrial Wastewaters by Sulfate Radical-Based Advanced Oxidation Processes (SR-AOPs). *Chem. Eng. J.* **2021**, *406*, 127083. [\[CrossRef\]](#)
3. Lin, D.; Fu, Y.; Li, X.; Wang, L.; Hou, M.; Hu, D.; Li, Q.; Zhang, Z.; Xu, C.; Qiu, S.; et al. Application of Persulfate-Based Oxidation Processes to Address Diverse Sustainability Challenges: A Critical Review. *J. Hazard. Mater.* **2022**, *440*, 129722. [\[CrossRef\]](#) [\[PubMed\]](#)
4. Honarmandrad, Z.; Sun, X.; Wang, Z.; Naushad, M.; Boczkaj, G. Activated Persulfate and Peroxymonosulfate Based Advanced Oxidation Processes (AOPs) for Antibiotics Degradation—A Review. *Water Resour. Ind.* **2023**, *29*, 100194. [\[CrossRef\]](#)
5. Qi, C.; Liu, X.; Ma, J.; Lin, C.; Li, X.; Zhang, H. Activation of Peroxymonosulfate by Base: Implications for the Degradation of Organic Pollutants. *Chemosphere* **2016**, *151*, 280–288. [\[CrossRef\]](#)
6. Li, J.; Liang, Y.; Jin, P.; Zhao, B.; Zhang, Z.; He, X.; Tan, Z.; Wang, L.; Cheng, X. Heterogeneous Metal-Activated Persulfate and Electrochemically Activated Persulfate: A Review. *Catalysts* **2022**, *12*, 1024. [\[CrossRef\]](#)
7. Wang, L.; Luo, D.; Hamdaoui, O.; Vasseghian, Y.; Momotko, M.; Boczkaj, G.; Kyzas, G.Z.; Wang, C. Bibliometric Analysis and Literature Review of Ultrasound-Assisted Degradation of Organic Pollutants. *Sci. Total Environ.* **2023**, *876*, 162551. [\[CrossRef\]](#)
8. Yang, L.; Xue, J.; He, L.; Wu, L.; Ma, Y.; Chen, H.; Li, H.; Peng, P.; Zhang, Z. Review on Ultrasound Assisted Persulfate Degradation of Organic Contaminants in Wastewater: Influences, Mechanisms and Prospective. *Chem. Eng. J.* **2019**, *378*, 122146. [\[CrossRef\]](#)

9. Fedorov, K.; Dinesh, K.; Sun, X.; Darvishi Cheshmeh Soltani, R.; Wang, Z.; Sonawane, S.; Boczkaj, G. Synergistic Effects of Hybrid Advanced Oxidation Processes (AOPs) Based on Hydrodynamic Cavitation Phenomenon—A Review. *Chem. Eng. J.* **2022**, *432*, 134191. [[CrossRef](#)]
10. Manos, D.; Papadopoulou, F.; Margellou, A.; Petrakis, D.; Konstantinou, I. Heterogeneous Activation of Persulfate by LaMO₃ (M = Co, Fe, Cu, Mn, Ni) Perovskite Catalysts for the Degradation of Organic Compounds. *Catalysts* **2022**, *12*, 187. [[CrossRef](#)]
11. Manz, K.E.; Kulaots, I.; Greenley, C.A.; Landry, P.J.; Lakshmi, K.V.; Woodcock, M.J.; Hellerich, L.; Bryant, J.D.; Apfelbaum, M.; Pennell, K.D. Low-Temperature Persulfate Activation by Powdered Activated Carbon for Simultaneous Destruction of Perfluorinated Carboxylic Acids and 1,4-Dioxane. *J. Hazard. Mater.* **2023**, *442*, 129966. [[CrossRef](#)] [[PubMed](#)]
12. Kemmou, L.; Frontistis, Z.; Vakros, J.; Manariotis, I.D.; Mantzavinos, D. Degradation of Antibiotic Sulfamethoxazole by Biochar-Activated Persulfate: Factors Affecting the Activation and Degradation Processes. *Catal. Today* **2018**, *313*, 128–133. [[CrossRef](#)]
13. Bekris, L.; Frontistis, Z.; Trakakis, G.; Sygellou, L.; Galiotis, C.; Mantzavinos, D. Graphene: A New Activator of Sodium Persulfate for the Advanced Oxidation of Parabens in Water. *Water Res.* **2017**, *126*, 111–121. [[CrossRef](#)] [[PubMed](#)]
14. Huang, W.; Xiao, S.; Zhong, H.; Yan, M.; Yang, X. Activation of Persulfates by Carbonaceous Materials: A Review. *Chem. Eng. J.* **2021**, *418*, 129297. [[CrossRef](#)]
15. Wu, Y.; Shi, Y.; Chen, H.; Zhao, J.; Dong, W. Activation of Persulfate by Magnetite: Implications for the Degradation of Low Concentration Sulfamethoxazole. *Process Saf. Environ. Prot.* **2018**, *116*, 468–476. [[CrossRef](#)]
16. Alexopoulou, C.; Petala, A.; Frontistis, Z.; Drivas, C.; Kennou, S.; Kondarides, D.I.; Mantzavinos, D. Copper Phosphide and Persulfate Salt: A Novel Catalytic System for the Degradation of Aqueous Phase Micro-Contaminants. *Appl. Catal. B Environ.* **2019**, *244*, 178–187. [[CrossRef](#)]
17. Xiong, Z.; Jiang, Y.; Wu, Z.; Yao, G.; Lai, B. Synthesis Strategies and Emerging Mechanisms of Metal–Organic Frameworks for Sulfate Radical-Based Advanced Oxidation Process: A Review. *Chem. Eng. J.* **2021**, *421*, 127863. [[CrossRef](#)]
18. Yuan, R.; Jiang, Z.; Wang, Z.; Gao, S.; Liu, Z.; Li, M.; Boczkaj, G. Hierarchical MnO₂ Nanoflowers Blooming on 3D Nickel Foam: A Novel Micro-Macro Catalyst for Peroxymonosulfate Activation. *J. Colloid Interface Sci.* **2020**, *571*, 142–154. [[CrossRef](#)]
19. Yuan, R.; Jiang, M.; Gao, S.; Wang, Z.; Wang, H.; Boczkaj, G.; Liu, Z.; Ma, J.; Li, Z. 3D Mesoporous α -Co(OH)₂ Nanosheets Electrodeposited on Nickel Foam: A New Generation of Macroscopic Cobalt-Based Hybrid for Peroxymonosulfate Activation. *Chem. Eng. J.* **2020**, *380*, 122447. [[CrossRef](#)]
20. Cao, J.; Lai, L.; Lai, B.; Yao, G.; Chen, X.; Song, L. Degradation of Tetracycline by Peroxymonosulfate Activated with Zero-Valent Iron: Performance, Intermediates, Toxicity and Mechanism. *Chem. Eng. J.* **2019**, *364*, 45–56. [[CrossRef](#)]
21. Yang, S.; Che, D. Degradation of Aquatic Sulfadiazine by Fe⁰/Persulfate: Kinetics, Mechanisms, and Degradation Pathway. *RSC Adv.* **2017**, *7*, 42233–42241. [[CrossRef](#)]
22. Wu, J.; Wang, B.; Blaney, L.; Peng, G.; Chen, P.; Cui, Y.; Deng, S.; Wang, Y.; Huang, J.; Yu, G. Degradation of Sulfamethazine by Persulfate Activated with Organo-Montmorillonite Supported Nano-Zero Valent Iron. *Chem. Eng. J.* **2019**, *361*, 99–108. [[CrossRef](#)]
23. Lei, Y.; Chen, C.-S.; Tu, Y.-J.; Huang, Y.-H.; Zhang, H. Heterogeneous Degradation of Organic Pollutants by Persulfate Activated by CuO-Fe₃O₄: Mechanism, Stability, and Effects of PH and Bicarbonate Ions. *Environ. Sci. Technol.* **2015**, *49*, 6838–6845. [[CrossRef](#)] [[PubMed](#)]
24. Zhao, W.; Shen, Q.; Nan, T.; Zhou, M.; Xia, Y.; Hu, G.; Zheng, Q.; Wu, Y.; Bian, T.; Wei, T.; et al. Cobalt-Based Catalysts for Heterogeneous Peroxymonosulfate (PMS) Activation in Degradation of Organic Contaminants: Recent Advances and Perspectives. *J. Alloys Compd.* **2023**, *958*, 170370. [[CrossRef](#)]
25. Li, B.; Wang, Y.-F.; Zhang, L.; Xu, H.-Y. Enhancement Strategies for Efficient Activation of Persulfate by Heterogeneous Cobalt-Containing Catalysts: A Review. *Chemosphere* **2022**, *291*, 132954. [[CrossRef](#)] [[PubMed](#)]
26. Zhang, T.; Chen, Y.; Wang, Y.; Le Roux, J.; Yang, Y.; Croué, J.-P. Efficient Peroxydisulfate Activation Process Not Relying on Sulfate Radical Generation for Water Pollutant Degradation. *Environ. Sci. Technol.* **2014**, *48*, 5868–5875. [[CrossRef](#)]
27. Du, X.; Zhang, Y.; Hussain, I.; Huang, S.; Huang, W. Insight into Reactive Oxygen Species in Persulfate Activation with Copper Oxide: Activated Persulfate and Trace Radicals. *Chem. Eng. J.* **2017**, *313*, 1023–1032. [[CrossRef](#)]
28. Jiang, L.; Xu, X.; Yuan, J.; Zuo, Y.; Tao, Y.; Yao, D.; He, G.; Chen, H. Heterogeneous Activation of Persulfate for the Degradation of Bisphenol A with Ni₂SnO₄-RGO. *New J. Chem.* **2020**, *44*, 6355–6361. [[CrossRef](#)]
29. Wu, Z.; Liang, Y.; Zou, D.; Yuan, X.; Xiao, Z.; Deng, Y.; Zhou, Y.; Jiang, L.; Qin, P. Enhanced Heterogeneous Activation of Persulfate by Ni_xCo_{3-x}O₄ for Oxidative Degradation of Tetracycline and Bisphenol A. *J. Environ. Chem. Eng.* **2020**, *8*, 104451. [[CrossRef](#)]
30. Kim, H.H.; Lee, D.; Choi, J.; Lee, H.; Seo, J.; Kim, T.; Lee, K.M.; Pham, A.L.T.; Lee, C. Nickel–Nickel Oxide Nanocomposite as a Magnetically Separable Persulfate Activator for the Nonradical Oxidation of Organic Contaminants. *J. Hazard. Mater.* **2020**, *388*, 121767. [[CrossRef](#)]
31. Liu, L.; Liu, Q.; Wang, Y.; Huang, J.; Wang, W.; Duan, L.; Yang, X.; Yu, X.; Han, X.; Liu, N. Nonradical Activation of Peroxydisulfate Promoted by Oxygen Vacancy-Laden NiO for Catalytic Phenol Oxidative Polymerization. *Appl. Catal. B Environ.* **2019**, *254*, 166–173. [[CrossRef](#)]
32. Xie, L.; Hao, J.; Xing, S. Enhanced Non-Radical Activation of Persulfate with Pompon-like NiO Microspheres for Removing Sulfamethoxazole in Water. *Environ. Sci. Pollut. Res. Int.* **2023**, *30*, 14455–14463. [[CrossRef](#)] [[PubMed](#)]
33. Huang, X.; Zhou, X.; Han, S.; Zhou, J.; Qian, G.; Gao, N. Cycle of Ni(II)-Ni(III)-Ni(II) in Ni-Doped Layered Double Hydroxides for Activation of Intercalated Peroxydisulfate. *Chem. Eng. J.* **2020**, *386*, 123937. [[CrossRef](#)]

34. Jian, S.; Sun, S.; Zeng, Y.; Liu, Z.; Liu, Y.; Yang, Q.; Ma, G. Highly Efficient Persulfate Oxidation Process Activated with NiO Nanosheets with Dominantly Exposed {1 1 0} Reactive Facets for Degradation of RhB. *Appl. Surf. Sci.* **2020**, *505*, 144318. [[CrossRef](#)]
35. Yue, D.; Guo, C.; Yan, X.; Wang, R.; Fang, M.; Wu, Y.; Qian, X.; Zhao, Y. Secondary Battery Inspired NiO Nanosheets with Rich Ni(III) Defects for Enhancing Persulfates Activation in Phenolic Waste Water Degradation. *Chem. Eng. J.* **2019**, *360*, 97–103. [[CrossRef](#)]
36. Gkika, C.; Petala, A.; Frontistis, Z.; Bampos, G.; Hela, D.; Konstantinou, I.; Mantzavinos, D. Heterogeneous Activation of Persulfate by Lanthanum Strontium Cobaltite for Sulfamethoxazole Degradation. *Catal. Today* **2021**, *361*, 130–138. [[CrossRef](#)]
37. Miao, J.; Sunarso, J.; Su, C.; Zhou, W.; Wang, S.; Shao, Z. SrCo_{1-x}Ti_xO_{3-δ} Perovskites as Excellent Catalysts for Fast Degradation of Water Contaminants in Neutral and Alkaline Solutions. *Sci. Rep.* **2017**, *7*, 44215. [[CrossRef](#)]
38. Wang, C.; Gao, S.; Zhu, J.; Xia, X.; Wang, M.; Xiong, Y. Enhanced Activation of Peroxydisulfate by Strontium Modified BiFeO₃ Perovskite for Ciprofloxacin Degradation. *J. Environ. Sci.* **2021**, *99*, 249–259. [[CrossRef](#)]
39. Cheng, C.; Gao, S.; Zhu, J.; Wang, G.; Wang, L.; Xia, X. Enhanced Performance of LaFeO₃ Perovskite for Peroxymonosulfate Activation through Strontium Doping towards 2,4-D Degradation. *Chem. Eng. J.* **2020**, *384*, 123377. [[CrossRef](#)]
40. Rodriguez-Mozaz, S.; Chamorro, S.; Marti, E.; Huerta, B.; Gros, M.; Sánchez-Melsió, A.; Borrego, C.M.; Barceló, D.; Balcázar, J.L. Occurrence of Antibiotics and Antibiotic Resistance Genes in Hospital and Urban Wastewaters and Their Impact on the Receiving River. *Water Res.* **2015**, *69*, 234–242. [[CrossRef](#)]
41. Song, Z.; Zhang, X.; Ngo, H.H.; Guo, W.; Wen, H.; Li, C. Occurrence, Fate and Health Risk Assessment of 10 Common Antibiotics in Two Drinking Water Plants with Different Treatment Processes. *Sci. Total Environ.* **2019**, *674*, 316–326. [[CrossRef](#)] [[PubMed](#)]
42. Cycoń, M.; Mrozik, A.; Piotrowska-Seget, Z. Antibiotics in the Soil Environment-Degradation and Their Impact on Microbial Activity and Diversity. *Front. Microbiol.* **2019**, *10*, 338. [[CrossRef](#)] [[PubMed](#)]
43. da Conceição, L.; Silva, A.M.; Ribeiro, N.F.P.; Souza, M.M.V.M. Combustion Synthesis of La_{0.7}Sr_{0.3}Co_{0.5}Fe_{0.5}O₃ (LSCF) Porous Materials for Application as Cathode in IT-SOFC. *Mater. Res. Bull.* **2011**, *46*, 308–314. [[CrossRef](#)]
44. Safakas, A.; Bampos, G.; Bebelis, S. Oxygen Reduction Reaction on La_{0.8}Sr_{0.2}Co_xFe_{1-x}O_{3-δ} Perovskite/Carbon Black Electrocatalysts in Alkaline Medium. *Appl. Catal. B Environ.* **2019**, *244*, 225–232. [[CrossRef](#)]
45. Petala, A.; Tsikritzis, D.; Kollia, M.; Ladas, S.; Kennou, S.; Kondarides, D.I. Synthesis and Characterization of N-Doped TiO₂ Photocatalysts with Tunable Response to Solar Radiation. *Appl. Surf. Sci.* **2014**, *305*, 281–291. [[CrossRef](#)]
46. Giannakopoulos, S.; Vakros, J.; Frontistis, Z.; Manariotis, I.D.; Venieri, D.; Pouloupoulos, S.G.; Mantzavinos, D. Biochar from Lemon Stalks: A Highly Active and Selective Carbocatalyst for the Oxidation of Sulfamethoxazole with Persulfate. *Catalysts* **2023**, *13*, 233. [[CrossRef](#)]
47. Li, M.; Bi, Y.-G.; Xiang, L.; Chen, X.-T.; Qin, Y.-J.; Mo, C.-H.; Zhou, S.-Q. Improved Cathodic Oxygen Reduction and Bioelectricity Generation of Electrochemical Reactor Based on Reduced Graphene Oxide Decorated with Titanium-Based Composites. *Bioresour. Technol.* **2020**, *296*, 122319. [[CrossRef](#)]
48. Wang, J.; Wei, Y.; Yang, B.; Wang, B.; Chen, J.; Jing, H. In Situ Grown Heterojunction of Bi₂WO₆/BiOCl for Efficient Photoelectrocatalytic CO₂ Reduction. *J. Catal.* **2019**, *377*, 209–217. [[CrossRef](#)]
49. Guo, P.-C.; Qiu, H.-B.; Yang, C.-W.; Zhang, X.; Shao, X.-Y.; Lai, Y.-L.; Sheng, G.-P. Highly Efficient Removal and Detoxification of Phenolic Compounds Using Persulfate Activated by MnO(x)@OMC: Synergistic Mechanism and Kinetic Analysis. *J. Hazard. Mater.* **2021**, *402*, 123846. [[CrossRef](#)]
50. Ding, S.; Wan, J.; Wang, Y.; Yan, Z.; Ma, Y. Activation of Persulfate by Molecularly Imprinted Fe-MOF-74 @ SiO₂ for the Targeted Degradation of Dimethyl Phthalate: Effects of Operating Parameters and Chlorine. *Chem. Eng. J.* **2021**, *422*, 130406. [[CrossRef](#)]
51. Qi, Y.; Zou, M.; Ajarem, J.S.; Allam, A.A.; Wang, Z.; Qu, R.; Zhu, F.; Huo, Z. Catalytic Degradation of Pharmaceutical and Personal Care Products in Aqueous Solution by Persulfate Activated with Nanoscale FeCoNi-Ternary Mixed Metal Oxides. *Sep. Purif. Technol.* **2023**, *314*, 123585. [[CrossRef](#)]
52. Sabri, M.; Habibi-Yangjeh, A.; Vadivel, S. Novel ZnO/Ag₆Si₂O₇ Nanocomposites for Activation of Persulfate Ions in Photocatalytic Removal of Organic Contaminants under Visible Light. *Mater. Chem. Phys.* **2020**, *239*, 121988. [[CrossRef](#)]
53. Liang, C.; Wang, Z.S.; Bruell, C.J. Influence of PH on Persulfate Oxidation of TCE at Ambient Temperatures. *Chemosphere* **2007**, *66*, 106–113. [[CrossRef](#)] [[PubMed](#)]
54. Matzek, L.W.; Carter, K.E. Activated Persulfate for Organic Chemical Degradation: A Review. *Chemosphere* **2016**, *151*, 178–188. [[CrossRef](#)] [[PubMed](#)]
55. Petala, A.; Arvaniti, O.S.; Christofili, M.; Safakas, A.; Frontistis, Z.; Mantzavinos, D. Lanthanum Nickel Oxide: An Effective Heterogeneous Activator of Sodium Persulfate for Antibiotics Elimination. *Catalysts* **2020**, *10*, 1373. [[CrossRef](#)]
56. Hong, Y.; Peng, J.; Zhao, X.; Yan, Y.; Lai, B.; Yao, G. Efficient Degradation of Atrazine by CoMgAl Layered Double Oxides Catalyzed Peroxymonosulfate: Optimization, Degradation Pathways and Mechanism. *Chem. Eng. J.* **2019**, *370*, 354–363. [[CrossRef](#)]
57. Wang, J.; Wang, S. Activation of Persulfate (PS) and Peroxymonosulfate (PMS) and Application for the Degradation of Emerging Contaminants. *Chem. Eng. J.* **2018**, *334*, 1502–1517. [[CrossRef](#)]
58. Ji, Y.; Fan, Y.; Liu, K.; Kong, D.; Lu, J. Thermo Activated Persulfate Oxidation of Antibiotic Sulfamethoxazole and Structurally Related Compounds. *Water Res.* **2015**, *87*, 1–9. [[CrossRef](#)]
59. Rønn, L.; Gydesen, E.; Bennedsen, L.R.; Muff, J.; Søgaard, E.G. Aalborg Universitet Influence of Chloride and Carbonates on the Reactivity of Activated Persulfate Chemosphere Influence of Chloride and Carbonates on the Reactivity of Activated Persulfate. *Chemosphere* **2012**, *86*, 1092–1097. [[CrossRef](#)]

60. Metheniti, M.; Frontistis, Z.; Ribeiro, R.; Silva, A.; Faria, J.; Gomes, H.; Mantzavinos, D. Degradation of Propyl Paraben by Activated Persulfate Using Iron-Containing Magnetic Carbon Xerogels: Investigation of Water Matrix and Process Synergy Effects. *Environ. Sci. Pollut. Res.* **2018**, *25*, 34801–34810. [[CrossRef](#)]
61. Oyekunle, D.T.; Cai, J.; Gendy, E.A.; Chen, Z. Chemosphere Impact of Chloride Ions on Activated Persulfates Based Advanced Oxidation Process (AOPs): A Mini Review. *Chemosphere* **2021**, *280*, 130949. [[CrossRef](#)] [[PubMed](#)]
62. Arvaniti, O.S.; Bairamis, F.; Konstantinou, I.; Mantzavinos, D.; Frontistis, Z. Degradation of Antihypertensive Drug Valsartan in Water Matrices by Heat and Heat/Ultrasound Activated Persulfate: Kinetics, Synergy Effect and Transformation Products. *Chem. Eng. J. Adv.* **2020**, *4*, 100062. [[CrossRef](#)]
63. Rayaroth, M.P.; Boczkaj, G.; Aubry, O.; Aravind, U.K.; Aravindakumar, C.T. Advanced Oxidation Processes for Degradation of Water Pollutants—Ambivalent Impact of Carbonate Species: A Review. *Water* **2023**, *15*, 1615. [[CrossRef](#)]
64. Feng, Y.; Song, Q.; Lv, W.; Liu, G. Degradation of Ketoprofen by Sulfate Radical-Based Advanced Oxidation Processes: Kinetics, Mechanisms, and Effects of Natural Water Matrices. *Chemosphere* **2017**, *189*, 643–651. [[CrossRef](#)]
65. Lee, H.; Kim, H.; Weon, S.; Choi, W.; Hwang, Y.S.; Seo, J.; Lee, C.; Kim, J.-H. Activation of Persulfates by Graphitized Nanodiamonds for Removal of Organic Compounds. *Environ. Sci. Technol.* **2016**, *50*, 10134–10142. [[CrossRef](#)]
66. Guo, R.; Xi, B.; Guo, C.; Liu, W.; Lv, N.; Xu, J. Comprehensive Insight into Heterogeneous Persulfate Activation for Environmental Pollutants Degradation: Approaches and Mechanism. *Environ. Funct. Mater.* **2022**, *1*, 239–252. [[CrossRef](#)]

Disclaimer/Publisher’s Note: The statements, opinions and data contained in all publications are solely those of the individual author(s) and contributor(s) and not of MDPI and/or the editor(s). MDPI and/or the editor(s) disclaim responsibility for any injury to people or property resulting from any ideas, methods, instructions or products referred to in the content.